miR-101a-3p overexpression prevents acetylcholine-$CaCl_2$-induced atrial fibrillation in rats via reduction of atrial tissue fibrosis, involving inhibition of EZH2

JING ZHU[1], NING ZHU[2] and JIAN XU[1]

[1]Department of Cardiology, The First Affiliated Hospital of USTC, Hefei, Anhui 230001;
[2]Department of Respiratory Medicine, Ningbo First Hospital, Ningbo, Zhejiang 315010, P.R. China

Received February 18, 2021; Accepted July 9, 2021

DOI: 10.3892/mmr.2021.12380

Abstract. Atrial fibrillation (AF), a clinically common heart arrhythmia, can result in left ventricular hypofunction, embolism and infarction. MicroRNA (miR)-101a-3p is lowly expressed in atrial tissues of patients with AF, but its role in AF remains unknown. In the present study, an AF model in rats was established via intravenous injection of acetylcholine (Ach)-$CaCl_2$. The downregulation of miR-101a-3p and upregulation of enhancer of zeste 2 homolog 2 (EZH2) were observed in AF model rats, indicating the involvement of miR-101a-3p and EZH2 in AF development. To study the effect of miR-101a-3p on AF *in vivo*, AF model rats were intramyocardially injected with lentivirus expressing miR-101a-3p. Electrocardiogram analysis identified that miR-101a-3p overexpression restored disappeared P wave and R-R interphase changes in Ach-$CaCl_2$-induced rats. Overexpression of miR-101a-3p also increased the atrial effective refractory period, reduced AF incidence and shortened duration of AF. Histological changes in atrial tissues were observed after H&E and Masson staining, which demonstrated that miR-101a-3p reduced atrial remodeling and fibrosis in AF model rats. Moreover, EZH2 expression was downregulated in atrial tissues by miR-101a-3p induction. Immunohistochemistry for collagen I and collagen III revealed a reduction in atrial collagen synthesis following miR-101a-3p overexpression in AF model rats. Additionally, miR-101a-3p lowered the expression of pro-fibrotic biomarkers, including TGF-β1, connective tissue growth factor, fibronectin and α-smooth muscle actin. The luciferase reporter assay results also indicated that EZH2 was a target gene of miR-101a-3p. Taken together, it was found that miR-101a-3p prevented AF in rats possibly via inhibition of collagen synthesis and atrial fibrosis by targeting EZH2, which provided a potential target for preventing AF.

Correspondence to: Dr Jian Xu, Department of Cardiology, The First Affiliated Hospital of USTC, 17 Lujiang Road, Luyang, Hefei, Anhui 230001, P.R. China
E-mail: zj_zkdyfy@126.com

Key words: atrial fibrillation, enhancer of zeste 2 homolog 2, fibrosis, microRNA-101a-3p, rats

Introduction

Atrial fibrillation (AF) is a cardiac arrhythmia in clinical settings with an increasing prevalence and estimated to affect >15 million individuals, which can result in left ventricular hypofunction, embolism and infarction (1-3). It is a progressive disease associated with a high mortality worldwide, and its onset and development are accompanied by atrial remodeling (4). Moreover, the influence of AF on human life is significant, and treating AF is associated with high expenses, thus exacerbating the socioeconomic burden of this disease (5). A characteristic of AF at the early stage is electrical remodeling, with a shortened atrial effective refractory period (AERP) and reduced physiological rate adaptation (5). Furthermore, in the late period, AF is manifested by structural remodeling and structural alterations such as atrial fibrosis (6). At present, treatment measures encompassing drug transfer, electric shock cardioversion, interventional therapy and surgical treatment are capable of restoring AF to sinus rhythm (2), but they lack efficacy.

MicroRNA (miRNA/miR), short non-coding RNA, modulates the translation of protein-coding genes by binding to the 3'untranslated regions (3'UTR) of mRNA (7). In the cardiovascular system, miRNA serves an important role in regulating a series of physiological functions in heart diseases, including cellular proliferation, apoptosis and differentiation (8). Accumulating evidence has shown the involvement of miRNAs in AF (9). For instance, miR-27b-3p overexpression controlled the Wnt/β-catenin signaling pathway by targeting Wnt3a, thereby relieving atrial fibrosis in rats with AF (10). Of note, miR-101 was found to be a regulatory factor in myocardial infarction, myocardial hypertrophy, rheumatic heart diseases and myocardial fibrosis (11-14). Previous studies have reported that overexpression of miR-101 could attenuate cardiac fibrosis and deterioration of cardiac function in rats after aortic constriction or coronary artery ligation (14,15). In addition, miR-101 expression was reported to be significantly downregulated in atrial samples from a canine model of AF and patients with AF (5).

EZH2 encodes a member of the polycomb-group family and exerts important roles in heart development and regeneration (16). An increase of EZH2 expression has been observed in atrial muscle and atrial fibroblasts of patients with AF (17). At the same time, inhibition of EZH2 mitigated the atrial enlargement and fibrosis induced by angiotensin II, and reduced the susceptibility of AF (17). Nevertheless, the detailed function of miR-101a-3p in atrial fibrosis triggered by AF has not been fully clarified.

In the current study, the AF model in rats was established as described in previous studies (10,18,19). The present study preliminarily investigated the effect of miR-101a-3p overexpression on the occurrence and development of AF via targeted regulation of EZH2. Given that both miR-101a-3p and EZH2 are closely associated with cardiac fibrosis (15,17), the role of miR-101a-3p overexpression in AF-mediated fibrosis was further examined. These results demonstrated that miR-101a-3p overexpression reduced atrial fibrosis by lowering the levels of collagen I, collagen III, TGF-β1, connective tissue growth factor (CTGF), fibronectin and α-smooth muscle actin (α-SMA). Moreover, it was verified that EZH2 was a target gene of miR-101a-3p. These findings provided insights for the prevention and treatment of AF.

Materials and methods

Experiment design. The animal experimental protocol was reviewed and approved by the Ethics Committee of The First Affiliated Hospital of USTC (approval no. 2019072014450004723 93). In total, 48 healthy male Sprague-Dawley rats (age, 8 weeks; weight, 200-250 g) were housed in under the following conditions: 22±1˚C, 45-55% humidity and 12 h light/12 h dark photoperiod and were given free access to food and water. A week after adaptation, rats were randomly assigned to four groups: Sham group, AF group, AF + lentivirus negative control (AF + LV-NC) group and AF + LV-miR-101a-3p group (n=12 each group).

293T cells were provided by Shanghai ZhongQiao XinZhou Biotechnology Co., Ltd. Cells in the logarithmic growth phase were co-transfected for 48 h with a second-generation lentivirus vector (pSico; Addgene, Inc.; 5 μg) and pHelper vector pMD2.G (Hunan Fenghui Biotechnology Co., Ltd.; 2 μg) and pHelper vector psPAX2 (Hunan Fenghui Biotechnology Co., Ltd.; 3 μg) using Lipofectamine 3000® reagent (cat. no. L3000015; Invitrogen; Thermo Fisher Scientific, Inc.) in the accordance with the manufacturer's protocol at 37˚C in an incubator containing 5% CO_2. Next, green fluorescent protein expression used for screening was observed under a fluorescence microscope at x100 magnification. Next, the supernatants were harvested via ultracentrifugation (72,000 x g) for 2 h at 4˚C and then stored at -80˚C.

For infection of LV vectors, rats were anesthetized with an intraperitoneal injection of pentobarbital sodium (50 mg/kg), immobilized, intubated and ventilated. After the breathing was stable, thoracic surgery was performed between the third and fourth intercostals space to expose the heart, and then 20 μl LV-NC or LV-miR-101a-3p (10^8 TU), based on the following sequences: miR-NC, 5'-TTCTCCGAACGTGTCACG TCGATTTCTCCGAACGTGTCACGTACCGGTTTCTCC GAACGTGTCACGTTCACTTCTCCGAACGTGTCACGT TTTTTT-3'; and miR-101a-3p, 5'-UACAGUACUGUGAUA ACUGAA-3', was injected into the right atrium of the rat, as described in previous studies (4,7). Sham rats and AF rats were injected with equal volume of saline. After 48 h from LV injection, all rats were anesthetized. Then, 1 ml/kg acetylcholine (Ach)-$CaCl_2$ mixture (cat. no. A6625; Sigma-Aldrich; Merck KGaA) containing 10 mg $CaCl_2$ and 60 μg Ach in mixture per ml ($CaCl_2$: Ach=1:0.006) was injected into rats via the tail vein daily for 7 days. Subsequently, the rats were euthanatized with an overdose (200 mg/kg) of pentobarbital sodium via intraperitoneal injection. The experimental design was displayed in Fig. 1A.

Electrocardiogram (ECG) recording. At day 8, rats from each group were anesthetized with pentobarbital sodium (50 mg/kg) via an intraperitoneal injection. Saline was given to sham rats, while others were given a mixture of Ach-$CaCl_2$ via the tail vein. Then, standard lead II ECG traces were recorded for evaluation of arrhythmias with 30-gauge subcutaneous needle electrodes (Grass Technologies) utilizing the BL-420F bio-function experiments system (Chengdu Techman Software Co., Ltd.; http://www.tme.com.cn/). With reference to a previous article (20), ECG signals were filtered (0.5-150 Hz) and amplified (20 mm/mV) with an FX8322 system (FUKUDA DENSHI). The sweep of ECG paper was performed at 50 mm/sec. Analog ECG recordings at baseline were made at 25-100 mm/sec paper speed and 1 mm/mV amplitude. Ach-$CaCl_2$ induced the absence of P waves, irregular heartbeat and R-R intervals from the ECG, which showed that the establishment of a rat AF model was successful (21).

Electrophysiological study. After AF induction, the rats were anesthetized with pentobarbital sodium, and the 2.0 F small animal electrophysiological catheter (Nippoly; https://www.nippoly.com/) was inserted by the jugular vein into the right atrial. The AERP was detected with S1-S2 programmed electrical stimulation (2X threshold at 2-msec duration) as previously reported (4). The S2 extra-stimulus method using eight regularly paced beats was delivered. AERP was measured at basic cycle lengths of 150 msec and was defined as the longest S1-S2 coupling interval failing to elicit an action potential. Moreover, AF duration was recorded, and AF inducibility was calculated. Finally, rats were sacrificed, and the atrial tissues were separated and stored at -70˚C or fixed at 4˚C in 4% paraformaldehyde until the following experiments.

H&E staining. Fixed atrial tissues of rats were dehydrated, embedded in paraffin and cut into 5-μm slices. The sections were deparaffinated and stained with hematoxylin (cat. no. H8070; Beijing Solarbio Science & Technology Co., Ltd.) for 5 min at room temperature. After being washed with distilled water, slices were counterstained with eosin at room temperature for 3 min. The pathological changes were visualized using a light microscope (BX53; Olympus Corporation) at x200 magnification.

Masson staining. A Masson staining kit (cat. no. DC0032; Beijing Leagene Biotechnology; http://www.leagene.com/) was employed to assess the degree of fibrosis in AF model rats according to the manufacturer's instructions. In brief,

dewaxed sections were stained with Reguad hematoxylin dye at room temperature for 6 min. The slices were immersed in 1% hydrochloric acid in ethanol for 3 sec and rinsed with distilled water for 2 min. Ponceau-acid fuchsin was added to each section and reacted for 1 min. After being washed with 0.2% glacial acetic acid, 1% phosphomolybdic acid was added and slices were counterstained with aniline blue for 5 min at room temperature, following which they were imaged under a light microscope. The size of fibrotic area was quantified as described in previous study (22). Digital images of five fields were randomly selected from each section and the mean of the fibrosis area of atrial tissues was calculated using Image-Pro Plus 6.0 analysis software (23,24).

Immunohistochemistry assay. Dewaxed slices were incubated with antigen retrieval solution (mixing 9 ml citrate buffer solution, 41 ml sodium citrate buffer solution and 450 ml distilled water; pH 6.0) for 10 min at 95˚C in a water bath. After being washed with PBS three times, the sections were incubated with 3% H_2O_2 (cat. no. 10011218; Sinopharm Chemical Reagent Co., Ltd.) for 15 min at room temperature and blocked with undiluted goat serum (cat. no. SL038; Beijing Solarbio Science & Technology Co., Ltd.) for 15 min at room temperature. Next, slices were incubated with antibodies against collagen I (cat. no. AF7001; 1:100; Affinity Biosciences), collagen III (cat. no. AF0136; 1:100; Affinity Biosciences) or EZH2 (cat. no. AF5150; 1:100; Affinity Biosciences) at 4˚C overnight. After being rinsed with PBS, sections were cultured with HRP-labeled goat anti-rabbit IgG (cat. no. 31460; 1:500; Thermo Fisher Scientific, Inc.) at 37˚C for 1 h. Diaminobenzidine (cat. no. DA1010; Beijing Solarbio Science & Technology Co., Ltd.) was added to each slice, and the sections were counterstained with hematoxylin for 3 min at room temperature. The staining results were observed with an Olympus light microscope at x400 magnification. Image-Pro Plus 6.0 software (23,24) was utilized for quantitative analysis. In total, three non-overlapping microscopic fields were selected and the number of positive-stained cells was counted. Finally, the mean value was calculated.

Reverse transcription-quantitative (RT-q)PCR. Total RNA was extracted from atrial tissues of rats using a commercial kit (cat. no. RP1201; BioTeke Corporation) according to the manufacturer's instructions. After detection of RNA purity and concentration, RNA was reverse transcribed into cDNA using the RNA Reverse Transcription kit (Takara Bio, Inc.). The reaction conditions were 37˚C for 30 min, 42˚C for 30 min and 70˚C for 10 min. For qPCR, cDNA templates, primers, SYBR GREEN (cat. no. EP1602; BioTeke Corporation) and Taq HS Perfect mix (cat. no. R300A; Takara Bio, Inc.) were mixed and incubated under standard PCR conditions. The reactions were incubated at 94˚C for 2 min, 94˚C for 10 sec, 60˚C for 15 sec and 72˚C for 15 sec, followed by 40 cycles at 72˚C for 5 min 30 sec, 40˚C for 5 min 30 sec, and melting from 60˚C to 94˚C, every 1˚C/1 sec, and 25˚C for 1 min. The expression level of miR-101a-3p was assessed using the $2^{-\Delta\Delta Cq}$ method (25). The primers utilized were supplied by GenScript, and their sequences were as follows: rno-miR-101a-3p forward, 5'-TACAGTACTGTGATAACTGAA-3' and reverse: 5'-GCAGGGTCCGAGGTATTC-3'; and 5S forward, 5'-GATCTCGGAAGCTAAGCAGG-3' and reverse, 5'-TGGTGCAGGGTCCGAGGTAT-3'.

Western blotting. The atrial tissues of rats were lysed in RIPA buffer (cat. no. P0013B; Beyotime Institute of Biotechnology) containing 1% PMSF (cat. no. ST506; Beyotime Institute of Biotechnology) on ice for 5 min. After centrifugation (4˚C, 10,000 x g, 3 min), the supernatants were collected as total protein samples. The concentration of protein was determined with a BCA kit (cat. no. P0009; Beyotime Institute of Biotechnology). The samples (30 μg protein) were separated via 10% SDS-PAGE at 80 V for 2.5 h and then transferred onto PVDF membranes (cat. no. LC2005; Thermo Fisher Scientific, Inc.). After reacting for 1.5 h at 80 V, the membranes were blocked with 5% BSA (cat. no. BS043, Biosharp Life Sciences) for 1 h at room temperature, and then incubated with primary antibody at 4˚C overnight. The membranes were cultured with secondary antibody for 40 min at 37˚C and washed with TBS-0.15% Tween 20. The bands were observed using a gel imaging system (WD-9413B, Beijing Liuyi Biotechnology Co., Ltd.) with ECL solution (cat. no. E003; 7 Sea Biotech). The information for the antibodies utilized in this study is as follows: EZH2 (85 kDa; cat. no. AF7901; 1:1,000, Affinity Biosciences), TGF-β1 (12 kDa; cat. no. BA0290; 1:1,000; Wuhan Boster Biological Technology, Ltd.), CTGF (38 kDa; cat. no. DF7091; 1:500; Affinity Biosciences), fibronectin (290 kDa; cat. no. A7488; 1:500; ABclonal Biotech Co., Ltd.), α-SMA (42 kDa; cat. no. AF1032; 1:500; Affinity Biosciences), β-actin (42 kDa; cat. no. 60008-1-Ig; 1:2,000; ProteinTech Group, Inc.), HRP-conjugated goat anti-rabbit IgG (cat. no. SA00001-2; 1:10,000; ProteinTech Group, Inc.) and HRP-conjugated goat anti-mouse IgG (cat. no. SA00001-1; 1:10,000; ProteinTech Group, Inc.).

Luciferase reporter gene assay. 293T cells were cultured with DMEM (cat. no. D5648; Sigma-Aldrich; Merck KGaA) containing 10% FBS (cat. no. F8067; Sigma-Aldrich; Merck KGaA) in an incubator (37˚C; 5% CO_2). The EZH2 wild-type (WT) sequences or mutant (MUT) sequences in 3'UTR containing the miR-101a-3p binding site were constructed and subcloned into the pmirGLO dual-luciferase miRNA target expression plasmid (GenScript), herein referred as EZH2 3'UTR WT or EZH2 3'UTR MUT. When the density reached 70%, the cells were seeded in a 12-well plate, and co-transfected with EZH2 3'UTR WT or MUT EZH2 3'UTR and miR-101a-3p mimics or mimics NC (JTS Scientific; http://www.jtsbio.com/) for 4 h in a saturated and humidified 37˚C incubator containing 5% CO_2. RNAs (75 pmol; 25 nmol/l) or plasmids (1.5 μg per well; 0.5 μg/ml) were transfected into 293T cells using Lipofectamine 2000® reagent (cat. no. 11668030; Invitrogen; Thermo Fisher Scientific, Inc.), following the manufacturer's instructions. Then, 48 h after transfection, cells were lysed and luciferase activity was measured using a Dual-Luciferase Reporter Assay system (cat. no. E1910; Promega Corporation). *Renilla* luciferase activity was utilized to normalize the reporter activity.

Statistical analysis. The data are presented as the mean ± standard deviation and were analyzed using GraphPad Prism 8 software (GraphPad Software, Inc.) with one-way ANOVA,

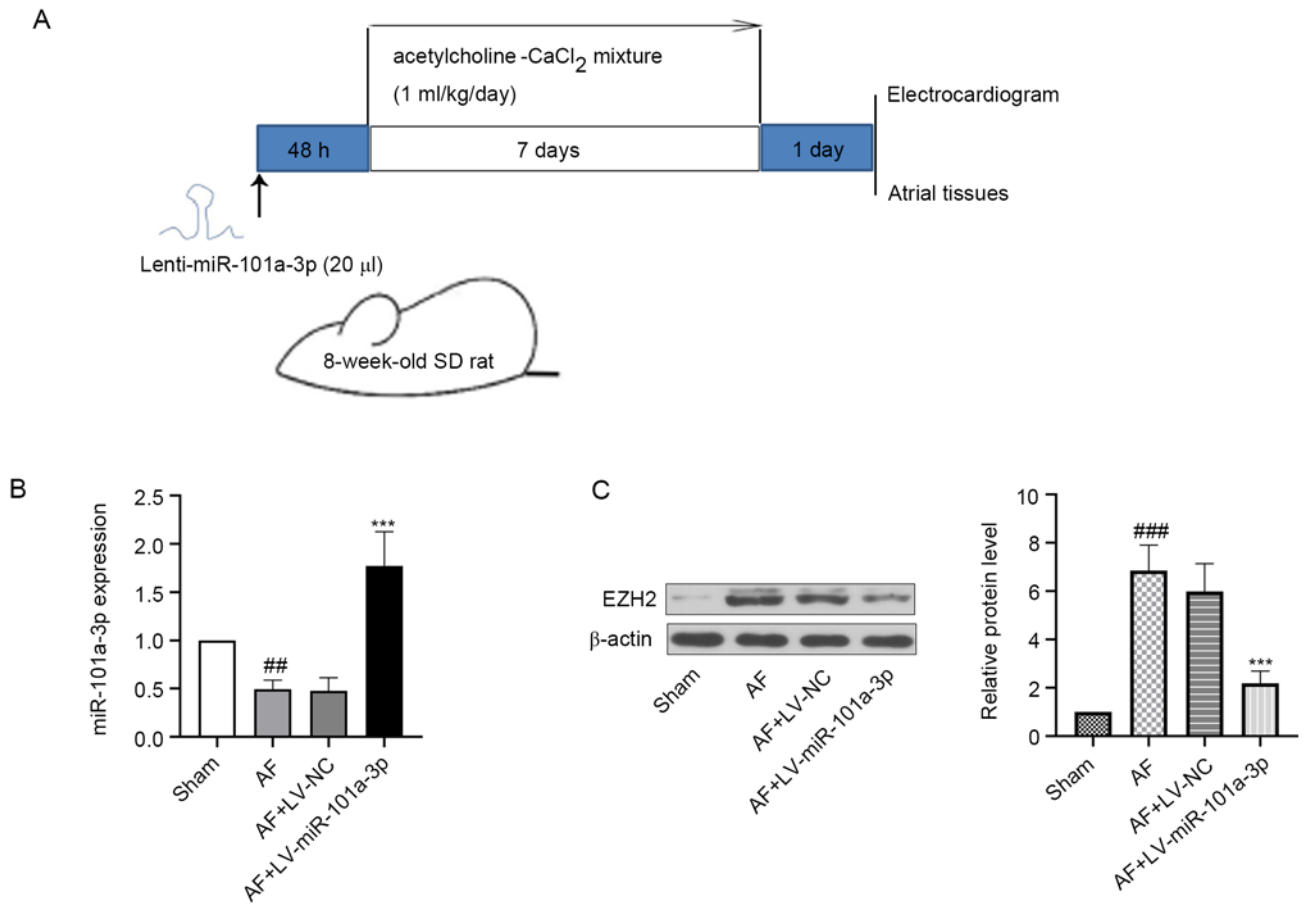

Figure 1. Expression levels of miR-101a-3p and EZH2 in atrial tissues of rats. The rats were anesthetized with an intraperitoneal injection of pentobarbital sodium (50 mg/kg), fixed, intubated and injected with LV-NC or LV-miR-101a-3p. After injection for 48 h, all rats were anesthetized. Then, 1 ml/kg acetylcholine-$CaCl_2$ mixture via the tail vein was injected into rats daily for 7 days. At day 8, rats were anesthetized, injected with Ach-$CaCl_2$ and sacrificed. The atrial tissues of heart were collected for following experiments. (A) Experimental protocol in rats. (B) miR-101a-3p expression was detected via reverse transcription-quantitative PCR. (C) Protein expression level of EZH2 was measured via western blotting. β-actin was used as an internal reference. The results are presented as the mean ± standard deviation (n=6). $^{\#\#}$P<0.01 and $^{\#\#\#}$P<0.001 vs. sham group; ***P<0.001 vs. AF + LV-NV group. LV-NC, lentivirus negative control; AF, atrial fibrillation; miR, microRNA; EZH2, enhancer of zeste 2 homolog 2; SD, Sprague-Dawley.

followed by Tukey's multiple comparisons test. All experiments were repeated independently ≥3 times. P<0.05 was considered to indicate a statistically significant difference.

Results

miR-101a-3p and EZH2 expression in atrial tissues of rats. The expression levels of miR-101a-3p and EZH2 in atrial tissues of AF model rats were evaluated using RT-qPCR and western blotting. It was found that miR-101a-3p expression was decreased in AF model rats when compared with the sham group. After infection with LV-miR-101a-3p, the expression level of miR-101a-3p was significantly increased (Fig. 1B). Moreover, it was suggested that the protein expression level of EZH2 was higher in the AF model group compared with that of sham rats (Fig. 1C). However, miR-101a-3p overexpression reduced EZH2 expression.

miR-101a-3p overexpression reduces the incidence and duration of AF in rats. To evaluate whether the AF model in rats was established successfully, electrophysiological changes were monitored. As shown in Fig. 2A, regular P wave was observed in the sham group, suggesting normal sinus rhythm. However, disappeared P wave and irregular R-R interphase changes were observed in AF model rats. In addition, a decreased heartbeat was observed in AF model rats, most likely owing to the continuous Ach-$CaCl_2$ perfusion. Interestingly, miR-101a-3p overexpression significantly inhibited heart rhythm changes in rats with AF. As presented in Fig. 2B, the AERP was shorter in AF model rats compared with that of sham rats. By contrast, miR-101a-3p overexpression reversed this process. Additionally, a lowered duration and incidence of AF was observed in AF + LV-miR-101a-3p group compared with AF model rats infected with LV-NC. These findings indicated the successful establishment of an AF rat model.

Pathological staining was performed to evaluate the severity of AF in rats. H&E staining was conducted to evaluate the pathological changes of atrial tissues in rats. As displayed in Fig. 3A, miR-101a-3p overexpression led to the reduction of Ach-$CaCl_2$-triggered tissue injury. Masson staining results also demonstrated that an increased degree of atrial fibrosis was observed in AF model rats, whereas miR-101a-3p overexpression abolished this process (Fig. 3B). The results of the quantitative analysis of fibrosis were consistent with that of Masson staining. Furthermore, immunohistochemistry

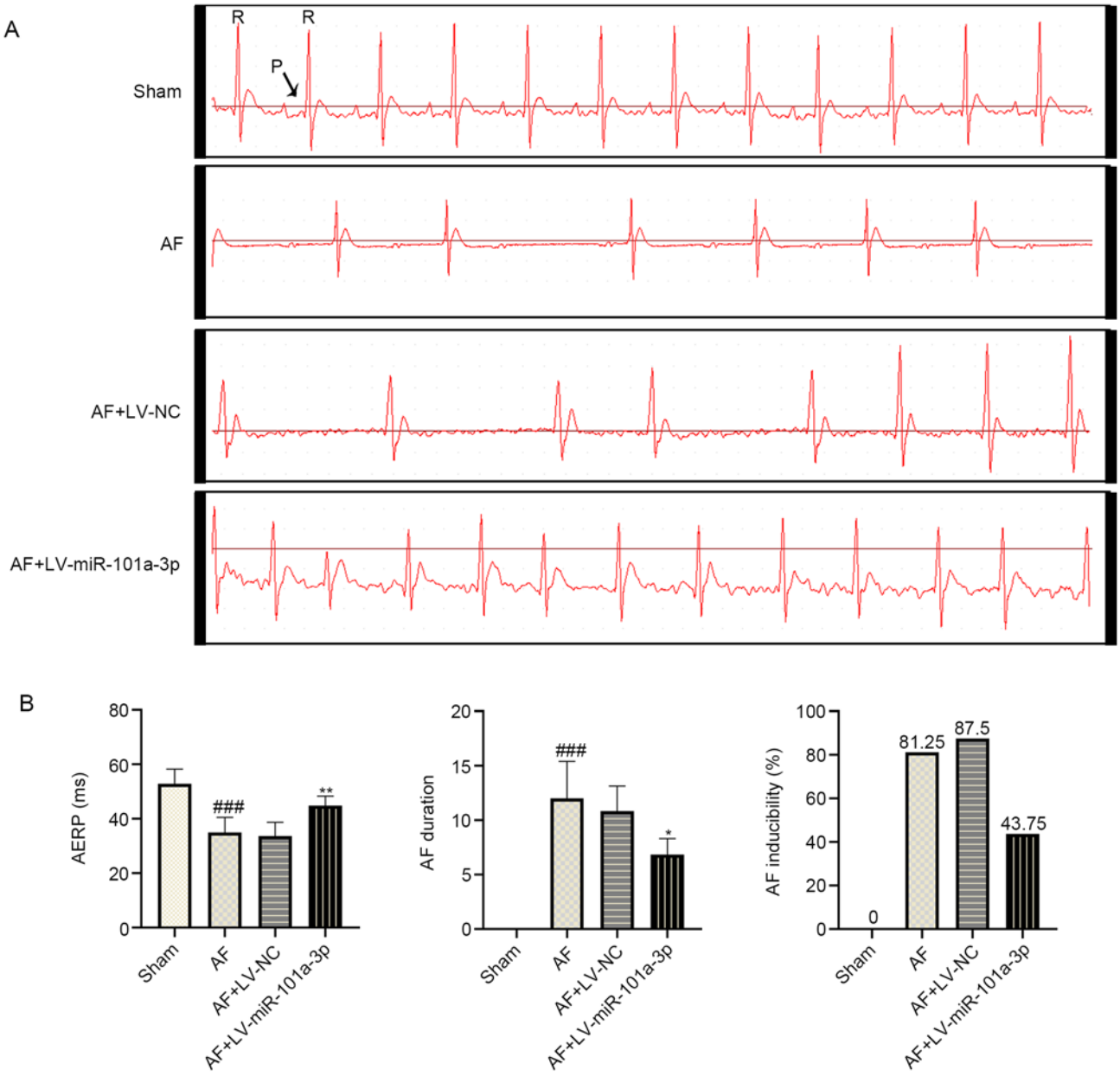

Figure 2. miR-101a-3p overexpression reduces the incidence and duration of AF in rats. (A) Changes in electrocardiogram were detected after AF induction. (B) AERP, AF duration and AF inducibility in rats were evaluated. The results are presented as the mean ± standard deviation (n=6). ###P<0.001 vs. sham group; *P<0.05 and **P<0.01 vs. AF + LV-NC group. AERP, atrial muscle effective refractory period; AF, atrial fibrillation; LV-NC, lentivirus negative control; miR, microRNA.

analysis confirmed that miR-101a-3p overexpression decreased the expression of EZH2 in atrial tissues (Fig. 3C).

miR-101a-3p overexpression attenuates atrial tissue fibrosis in rats with AF. To further examine the role of miR-101a-3p overexpression in tissue fibrosis, the changes of collagen I and collagen III were detected. As shown in Fig. 4A and B, Ach-$CaCl_2$ significantly increased atrial fibrosis by upregulating collagen I and collagen III expression. On the contrary, miR-101a-3p overexpression decreased these protein expression levels. In addition, the western blotting results indicated that Ach-$CaCl_2$-induced AF significantly increased the expression levels of TGF-β1, CTGF, fibronectin and α-SMA, which were downregulated by miR-101a-3p overexpression (Fig. 4C).

miR-101a-3p can bind to EZH2 3'UTR. Next, the relationship between miR-101a-3p and EZH2 was evaluated. The binding sequences of miR-101a-3p and EZH2 (WT or MUT) are presented in Fig. 5A. After co-transfection for 48 h, luciferase activity was assessed. Of note, the luciferase activity in EZH2 3'UTR WT + miR-101a-3p mimics group was decreased in comparison with MUT EZH2 3'UTR + miR-101a-3p mimics group (Fig. 5B). This result demonstrated that EZH2 was one of the target genes of miR-101a-3p.

Discussion

The aim of the present study was to evaluate the effect of miR-101a-3p overexpression on atrial fibrosis in Ach-$CaCl_2$-induced AF model rats. The results suggested that

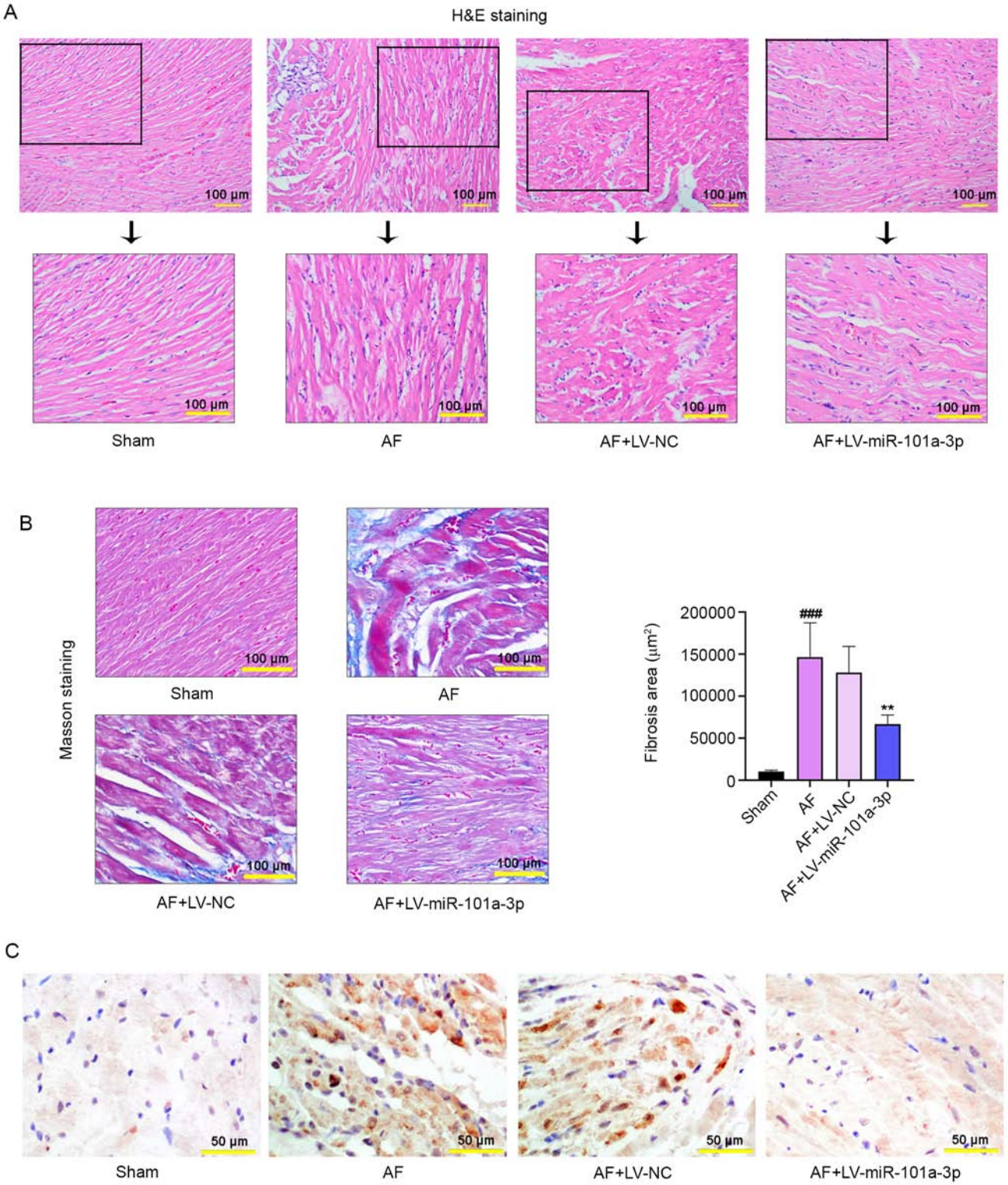

Figure 3. Pathological staining for evaluating the severity of AF in rats. (A) The atrial tissues of heart were stained with H&E and observed using a microscope. Scale bar, 100 μm. (B) Masson staining was employed to evaluate tissue fibrosis and the results were quantified accordingly. Scale bar, 100 μm. (C) Immunohistochemistry assay was utilized to examine EZH2 expression in atrial tissues. Scale bar, 50 μm. Data are expressed as the mean ± standard deviation (n=6). $^{###}$P<0.001 vs. sham group; **P<0.01 vs. AF + LV-NC group. AF, atrial fibrillation; LV-NC, lentivirus negative control; miR, microRNA.

miR-101a-3p expression was downregulated and the protein expression level of EZH2 was upregulated in atrial tissues of AF model rats. On the contrary, miR-101a-3p overexpression increased the expression level of miR-101a-3p but decreased EZH2 expression. Additionally, Ach-$CaCl_2$-induced tissue injury was significantly reduced by overexpression of miR-101a-3p.

At present, researchers have reported that AF can be induced either pharmacologically or by vagal stimulation (26). For example, Zhang *et al* (27) revealed that AF was induced by infusion of angiotensin II (2,000 ng/kg per min) for 3 weeks in male C57BL/6 mice. Moreover, Zou *et al* (18) reported that 1 ml/kg Ach-$CaCl_2$ exposure results in the absence of P

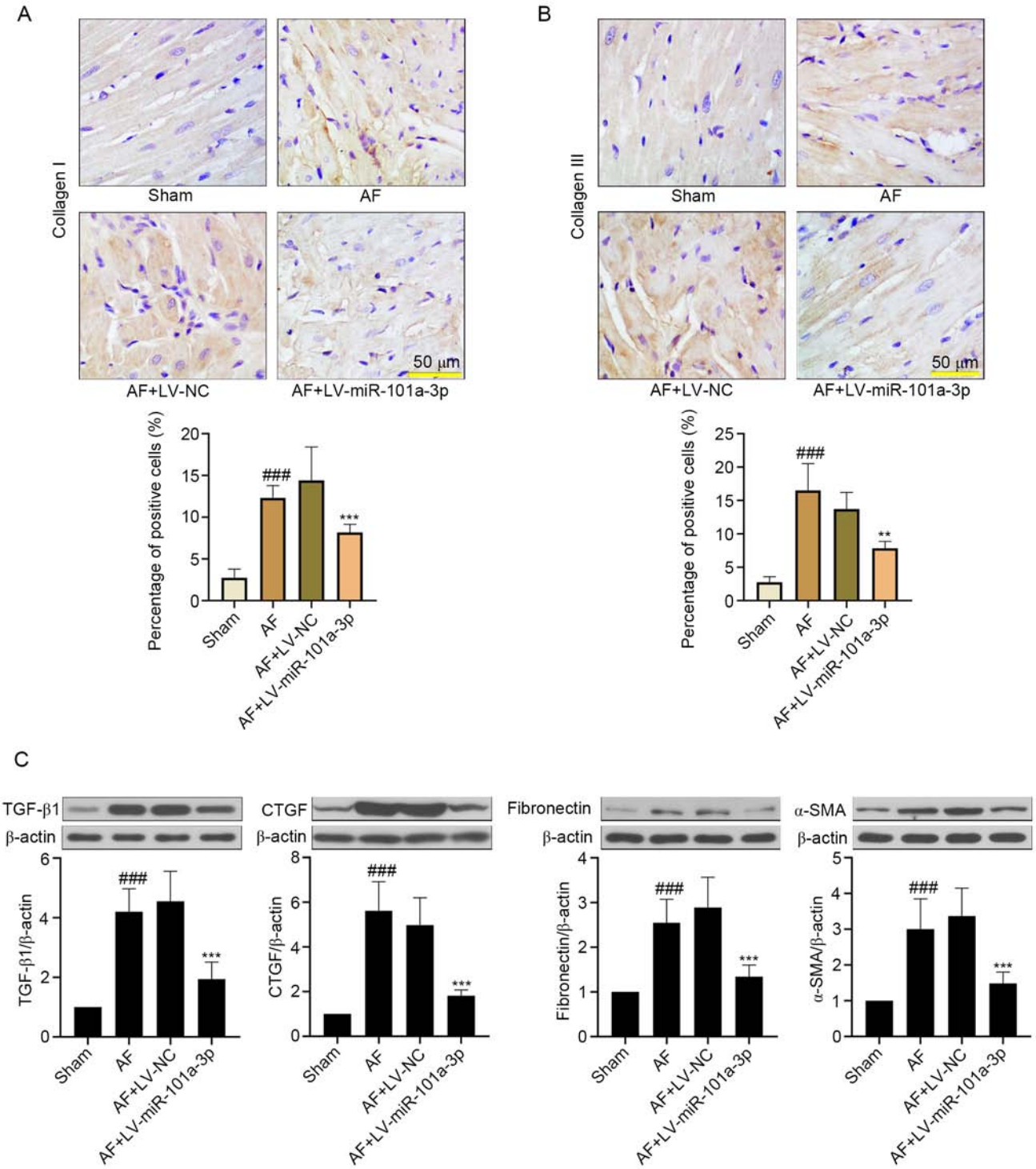

Figure 4. miR-101a-3p overexpression attenuates atrial tissue fibrosis in rats with AF. Expression levels of (A) collagen I and (B) collagen III in atrial tissues of heart were determined via immunohistochemistry. At the same time, quantitative analysis was carried out. (C) Protein expression levels of TGF-β1, CTGF, fibronectin and α-SMA in atrial tissues of heart were assessed via western blotting. The results are presented as the mean ± standard deviation (n=6). ###P<0.001 vs. sham group; **P<0.01 and ***P<0.001 vs. AF + LV-NC group. CTGF, connective tissue growth factor; α-SMA, α-smooth muscle actin; AF, atrial fibrillation; LV-NC, lentivirus negative control; miR, microRNA.

waves, irregular heartbeat and R-R intervals from the ECG, indicating the successful establishment of the AF model. Thus, in our present study, an AF model in rats was established by Ach-$CaCl_2$ injection via the tail vein. Atrial fibrosis is one of the main manifestations in the progression of AF. In the present study, Masson staining was conducted to assess the degree of atrial tissue fibrosis. It was found that AF-mediated tissue fibrosis in rats was inhibited by miR-101a-3p overexpression, which was in agreement with a previous study (10). Moreover, the accumulation of extracellular matrix (ECM) proteins, such as collagen I and collagen III, is able to enhance tissue stiffness and cause cardiac diastolic dysfunction (28). As reported by Wang *et al* (29), long non-coding RNA NRON, functioned as a nuclear factor of activated T cells repressor, improved

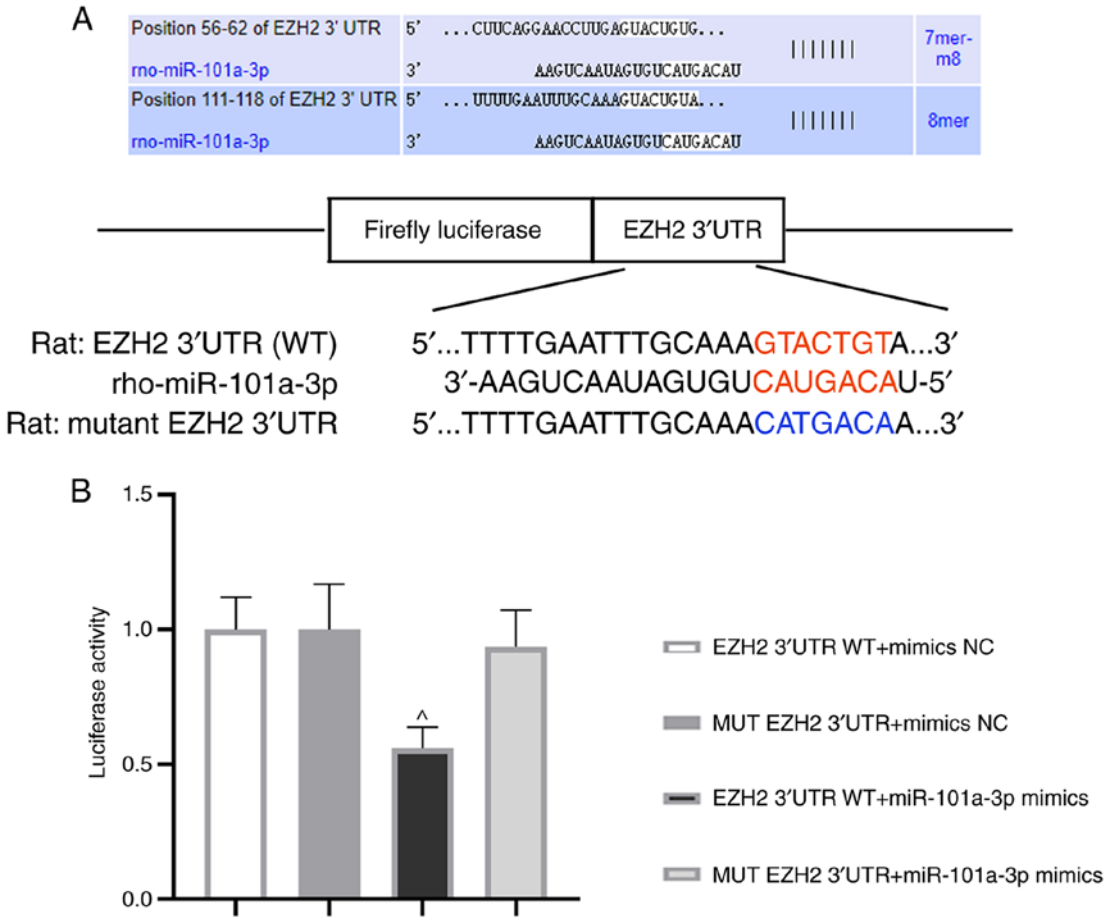

Figure 5. EZH2 is a target gene of miR-101a-3p. (A) Binding sequences of miR-101a-3p and EZH2 (WT or MUT) in rats. (B) 293T cells were co-transfected with EZH2 3'UTR WT or MUT EZH2 3'UTR and miR-101a-3p mimics or mimics NC. After transfection for 48 h, luciferase activity was measured using the corresponding kit. The results are expressed as the mean ± standard deviation (n=3). ^P<0.05 vs. MUT EZH2 3'UTR + miR-101a-3p mimics group. WT, wild-type; MUT, mutant type; NC, negative control; UTR, untranslated region; miR, microRNA; EZH2, enhancer of zeste 2 homolog 2.

atrial fibrosis via a reduction of collagen I and collagen III expression. Consistent with the previous study, the current experiments indicated that miR-101a-3p overexpression lowered these protein expression levels, as determined by immunohistochemistry staining. In order to further investigate the underlying mechanisms of atrial fibrosis, the present study also detected the changes in the protein expression levels of TGF-β1, CTGF, fibronectin and α-SMA. Among them, TGF-β serves a crucial role in the development of fibrosis, especially TGF-β1 existing in multi-tissues (15). CTGF, a downstream factor of TGF-β1, has been considered a secreted protein and can facilitate the synthesis of ECM (30). Similarly, excessive fibronectin and α-SMA generation is a hallmark of atrial fibrosis (31,32). In the present study, increased TGF-β1, CTGF, fibronectin and α-SMA expression was observed in the AF group. By contrast, the overexpression of miR-101a-3p reversed these protein expression levels. To the best of our knowledge, this finding that miR-101a-3p overexpression reduced atrial fibrosis in rats administrated with Ach-$CaCl_2$ via a decrease of these biomarker protein expressions has not been reported previously.

EZH2 is a histone-lysine N-methyltransferase enzyme, participating in histone methylation. In recent years, it has been reported that dysregulation of EZH2 is closely involved in the pathogenesis and development of various cancer types, such as hepatocellular carcinoma, head and neck cancer and triple-negative breast cancer (33-35). It is well-known that EZH2 has a vital role in modulation of cell differentiation (17). As evidenced by Xiao *et al* (36), EZH2 promoted the differentiation of pulmonary fibroblasts to myofibroblasts by facilitating the nuclear translocation of Smad2/3. Moreover, EZH2 is responsible for regulating wound healing, fibrogenesis and epithelial-mesenchymal transition (EMT) (37). A previous study indicated that miR-214-3p suppressed fibrotic phenotype in cardiac myofibroblasts by decreasing EZH2 expression (38). Another study reported that EZH2 triggered EMT in endometriosis (37). Additionally, it was shown that EZH2 was a target gene of miR-101 and the downregulation of miR-101 expression in cancer resulted in EZH2 overexpression, thereby affecting cancer progression (36). Similar to the previous study, the current luciferase assay results demonstrated that EZH2 was one of the target genes of miR-101a-3p. However, whether miR-101a-3p attenuated atrial fibrosis induced by AF via regulation of EZH2 remains unknown and it is worthy of research in the future.

Accumulating evidence has revealed the critical roles of EZH2 in inducing tissue and organ fibrosis (39). Fibrosis aggravates the pathogenesis of a variety of chronic disorders that affects the liver, renal, lung and heart (40). Recently, the role of EZH2 in renal fibrosis, liver fibrosis and peritoneal fibrosis has been investigated (39-41). However, its effect

on atrial fibrosis in Ach-$CaCl_2$-administrated rats and the underlying mechanisms are not fully understood. The present study found that the protein expression level of EZH2 was increased, while miR-101a-3p overexpression decreased EZH2 expression in AF model rats, and miR-101a-3p overexpression attenuated AF-initiated atrial fibrosis (Fig. S1). Although the present study assessed the role of miR-101a-3p overexpression in AF, the detailed molecular mechanisms are yet to be fully elucidated. Therefore, targeting signaling pathways associated with AF-induced atrial fibrosis is necessary. Emerging studies have shown that the Wnt/β-catenin signaling pathway serves an important part in regulation of EMT and has been considered as an effective therapeutic strategy for fibrosis (39,42,43). Inhibition of EZH2 mitigated angiotensin II-mediated fibroblast activation via the TGF-β-Smad signaling pathway (17). Moreover, the NF-κB signaling pathway is closely correlated with cardiac remodeling (17). As such, the aforementioned signaling pathways deserve careful study in the future.

miRNAs can degrade or block the translation of the target mRNA to suppress gene expression, while delivering these RNAs to specific cells, which presents a significant challenge due to widespread off-targeting (44,45). In the current study, miR-101a-3p overexpression induced by a lentivirus significantly upregulated miR-101a-3p expression and downregulated that of EZH2 in atrial tissues of AF model rats. It was identified that overexpression of miR-101a-3p effectively reduced atrial fibrosis and mitigated AF. Moreover, EZH2 was a target gene of miR-101a-3p. These data demonstrated that lentivirus-mediated miR-101a-3p, delivered via intramyocardial injection, affected EZH2 expression in atrial tissues, thereby modulating the atrial fibrosis of rats. Although it is necessary to further examine whether there is off-target blockage of EZH2 in multiple bystander cells, the present study identified the effect of miR-101a-3p/EZH2 axis on AF model rats. In addition, AF was induced by injection of Ach-$CaCl_2$, which was in accordance with previous studies (18,26). However, the majority of human AF may not be Ach-$CaCl_2$-induced AF. Therefore, the development a novel animal model to better mimic human AF is necessary for further research of the clinical implications.

In summary, the present results demonstrated that miR-101a-3p expression was downregulated in AF model rats. In addition, the *in vivo* investigations revealed that the overexpression of miR-101a-3p mitigated AF by reducing atrial fibrosis, suggesting that miR-101a-3p may be a potential target for preventing and treating AF.

Acknowledgements

Not applicable.

Funding

No funding was received.

Availability of data and materials

The datasets used and/or analyzed during the current study are available from the corresponding author on reasonable request.

Authors' contributions

JZ and JX conceptualized the study and designed the experiments. JZ and NZ performed the experiments. JZ and NZ analyzed the data and guaranteed the authenticity of the raw data. JZ wrote the paper. JX revised the manuscript. All authors read and approved the final manuscript.

Ethics approval and consent to participate

All animal procedures were approved by the Ethics Committee of The First Affiliated Hospital of USTC (Hefei, China; approval no. 20190720144500047239 3).

Patient consent for publication

Not applicable.

Competing interests

The authors declare that they have no competing interests.

References

1. Yan Y, Shi R, Yu X, Sun C, Zang W and Tian H: Identification of atrial fibrillation-associated microRNAs in left and right atria of rheumatic mitral valve disease patients. Genes Genet Syst 94: 23-34, 2019.
2. Ferrari R, Bertini M, Blomstrom-Lundqvist C, Dobrev D, Kirchhof P, Pappone C, Ravens U, Tamargo J, Tavazzi L and Vicedomini GG: An update on atrial fibrillation in 2014: From pathophysiology to treatment. Int J Cardiol 203: 22-29, 2016.
3. Carapetis JR, Steer AC, Mulholland EK and Weber M: The global burden of group A streptococcal diseases. Lancet Infect Dis 5: 685-694, 2005.
4. Yao L, Zhou B, You L, Hu H and Xie R: LncRNA MIAT/miR-133a-3p axis regulates atrial fibrillation and atrial fibrillation-induced myocardial fibrosis. Mol Biol Rep 47: 2605-2617, 2020.
5. Lu Y, Zhang Y, Wang N, Pan Z, Gao X, Zhang F, Zhang Y, Shan H, Luo X, Bai Y, *et al*: MicroRNA-328 contributes to adverse electrical remodeling in atrial fibrillation. Circulation 122: 2378-2387, 2010.
6. Santulli G, Iaccarino G, De Luca N, Trimarco B and Condorelli G: Atrial fibrillation and microRNAs. Front Physiol 5: 15, 2014.
7. Li X, Wang B, Cui H, Du Y, Song Y, Yang L, Zhang Q, Sun F, Luo D, Xu C, *et al*: Let-7e replacement yields potent anti-arrhythmic efficacy via targeting beta 1-adrenergic receptor in rat heart. J Cell Mol Med 18: 1334-1343, 2014.
8. Galenko O, Jacobs V, Knight S, Taylor M, Cutler MJ, Muhlestein JB, Carlquist JL, Knowlton KU and Jared Bunch T: The role of microRNAs in the development, regulation, and treatment of atrial fibrillation. J Interv Card Electrophysiol 55: 297-305, 2019.
9. Briasoulis A, Sharma S, Telila T, Mallikethi-Reddy S, Papageorgiou N, Oikonomou E and Tousoulis D: MicroRNAs in atrial fibrillation. Curr Med Chem 26: 855-863, 2019.
10. Lv X, Li J, Hu Y, Wang S, Yang C, Li C and Zhong G: Overexpression of miR-27b-3p targeting Wnt3a regulates the signaling pathway of Wnt/β-catenin and attenuates atrial fibrosis in rats with atrial fibrillation. Oxid Med Cell Longev 2019: 5703764, 2019.
11. Li Q, Gao Y, Zhu J and Jia Q: MiR-101 attenuates myocardial infarction-induced injury by targeting DDIT4 to regulate autophagy. Curr Neurovasc Res 17: 123-130, 2020.
12. Xiao L, Gu Y, Sun Y, Chen J, Wang X, Zhang Y, Gao L and Li L: The long noncoding RNA XIST regulates cardiac hypertrophy by targeting miR-101. J Cell Physiol 234: 13680-13692, 2019.
13. Dong H, Sun Y, Shan F, Sun Q and Yang B: Down-regulation of miR-101 contributes to rheumatic heart disease through up-regulating TLR2. Med Sci Monit 21: 1500-1506, 2015.

14. Pan Z, Sun X, Shan H, Wang N, Wang J, Ren J, Feng S, Xie L, Lu C, Yuan Y, *et al*: MicroRNA-101 inhibited postinfarct cardiac fibrosis and improved left ventricular compliance via the FBJ osteosarcoma oncogene/transforming growth factor-β1 pathway. Circulation 126: 840-850, 2012.
15. Zhou Y, Shiok TC, Richards AM and Wang P: MicroRNA-101a suppresses fibrotic programming in isolated cardiac fibroblasts and in vivo fibrosis following trans-aortic constriction. J Mol Cell Cardiol 121: 266-276, 2018.
16. Ai S, Yu X, Li Y, Peng Y, Li C, Yue Y, Tao G, Li C, Pu WT and He A: Divergent requirements for EZH1 in heart development versus regeneration. Circ Res 121: 106-112, 2017.
17. Song S, Zhang R, Mo B, Chen L, Liu L, Yu Y, Cao W, Fang G, Wan Y, Gu Y, *et al*: EZH2 as a novel therapeutic target for atrial fibrosis and atrial fibrillation. J Mol Cell Cardiol 135: 119-133, 2019.
18. Zou D, Geng N, Chen Y, Ren L, Liu X, Wan J, Guo S and Wang S: Ranolazine improves oxidative stress and mitochondrial function in the atrium of acetylcholine-$CaCl_2$ induced atrial fibrillation rats. Life Sci 156: 7-14, 2016.
19. Yang Q, Lv Q, Feng M, Liu M, Feng Y, Lin S, Yang J and Hu J: Taurine prevents the electrical remodeling in Ach-CaCl(2) induced atrial fibrillation in rats. Adv Exp Med Biol 975: 821-830, 2017.
20. Zhou Q, Chen B, Chen X, Wang Y, Ji J, Kizaibek M, Wang X, Wu L, Hu Z, Gao X, *et al*: Arnebiae Radix prevents atrial fibrillation in rats by ameliorating atrial remodeling and cardiac function. J Ethnopharmacol 248: 112317, 2020.
21. Li Y, Song B and Xu C: Effects of Guanfu total base on Bcl-2 and Bax expression and correlation with atrial fibrillation. Hellenic J Cardiol 59: 274-278, 2018.
22. Wang Z, Ouyang Q, Huang Z, Lin L, Yu E and Ferrari MW: Prenatal nicotine exposure induces gender-associated left ventricular-arterial uncoupling in adult offspring. Mol Med Rep 12: 410-418, 2015.
23. Chen B, Xu M and Li B: The clinical experience for treating post-burn depigmentation with tiny epidermal particles graft. Int Wound J 14: 165-171, 2017.
24. Wang C, Yuan W, Hu A, Lin J, Xia Z, Yang CF, Li Y and Zhang Z: Dexmedetomidine alleviated sepsis-induced myocardial ferroptosis and septic heart injury. Mol Med Rep 22: 175-184, 2020.
25. Livak KJ and Schmittgen TD: Analysis of relative gene expression data using real-time quantitative PCR and the 2(-Delta Delta C(T)) method. Methods 25: 402-408, 2001.
26. Gaspo R: The tachycardia-induced dog model of atrial fibrillation. clinical relevance and comparison with other models. J Pharmacol Toxicol Methods 42: 11-20, 1999.
27. Zhang YL, Cao HJ, Han X, Teng F, Chen C, Yang J, Yan X, Li PB, Liu Y, Xia YL, *et al*: Chemokine receptor CXCR-2 initiates atrial fibrillation by triggering monocyte mobilization in mice. Hypertension 76: 381-392, 2020.
28. Dong Q, Li S, Wang W, Han L, Xia Z, Wu Y, Tang Y, Li J and Cheng X: FGF23 regulates atrial fibrosis in atrial fibrillation by mediating the STAT3 and SMAD3 pathways. J Cell Physiol 234: 19502-19510, 2019.
29. Wang Y, Xu P, Zhang C, Feng J, Gong W, Ge S and Guo Z: LncRNA NRON alleviates atrial fibrosis via promoting NFATc3 phosphorylation. Mol Cell Biochem 457: 169-177, 2019.
30. Qiao G, Xia D, Cheng Z and Zhang G: miR-132 in atrial fibrillation directly targets connective tissue growth factor. Mol Med Rep 16: 4143-4150, 2017.
31. Chen X, Zhang W, Wang Q, Du L, Yi Y, Liu Y, Liu X and Duan S: Eplerenone inhibits atrial fibrosis in mutant TGF-β1 transgenic mice. Sci China Life Sci 59: 1042-1047, 2016.
32. Burstein B, Qi XY, Yeh YH, Calderone A and Nattel S: Atrial cardiomyocyte tachycardia alters cardiac fibroblast function: A novel consideration in atrial remodeling. Cardiovasc Res 76: 442-452, 2007.
33. Xiao G, Jin LL, Liu CQ, Wang YC, Meng YM, Zhou ZG, Chen J, Yu XJ, Zhang YJ, Xu J and Zheng L: EZH2 negatively regulates PD-L1 expression in hepatocellular carcinoma. J Immunother Cancer 7: 300, 2019.
34. Zhou L, Mudianto T, Ma X, Riley R and Uppaluri R: Targeting EZH2 enhances antigen presentation, antitumor immunity, and circumvents Anti-PD-1 resistance in head and neck cancer. Clin Cancer Res 26: 290-300, 2020.
35. Yomtoubian S, Lee SB, Verma A, Izzo F, Markowitz G, Choi H, Cerchietti L, Vahdat L, Brown KA, Andreopoulou E, *et al*: Inhibition of EZH2 catalytic activity selectively targets a metastatic subpopulation in triple-negative breast cancer. Cell Rep 30: 755-770.e6, 2020.
36. Xiao X, Senavirathna LK, Gou X, Huang C, Liang Y and Liu L: EZH2 enhances the differentiation of fibroblasts into myofibroblasts in idiopathic pulmonary fibrosis. Physiol Rep 4: e12915, 2016.
37. Zhang Q, Dong P, Liu X, Sakuragi N and Guo SW: Enhancer of Zeste homolog 2 (EZH2) induces epithelial-mesenchymal transition in endometriosis. Sci Rep 7: 6804, 2017.
38. Zhu WS, Tang CM, Xiao Z, Zhu JN, Lin QX, Fu YH, Hu ZQ, Zhang Z, Yang M, Zheng XL, *et al*: Targeting EZH1 and EZH2 contributes to the suppression of fibrosis-associated genes by miR-214-3p in cardiac myofibroblasts. Oncotarget 7: 78331-78342, 2016.
39. Zhou X, Xiong C, Tolbert E, Zhao TC, Bayliss G and Zhuang S: Targeting histone methyltransferase enhancer of zeste homolog-2 inhibits renal epithelial-mesenchymal transition and attenuates renal fibrosis. FASEB J 32: fj201800237R, 2018.
40. Cai X, Li Z, Zhang Q, Qu Y, Xu M, Wan X and Lu L: CXCL6-EGFR-induced Kupffer cells secrete TGF-β1 promoting hepatic stellate cell activation via the SMAD2/BRD4/C-MYC/EZH2 pathway in liver fibrosis. J Cell Mol Med 22: 5050-5061, 2018.
41. Shi Y, Tao M, Wang Y, Zang X, Ma X, Qiu A, Zhuang S and Liu N: Genetic or pharmacologic blockade of enhancer of zeste homolog 2 inhibits the progression of peritoneal fibrosis. J Pathol 250: 79-94, 2020.
42. Gonzalez DM and Medici D: Signaling mechanisms of the epithelial-mesenchymal transition. Sci Signal 7: re8, 2014.
43. Duan J, Gherghe C, Liu D, Hamlett E, Srikantha L, Rodgers L, Regan JN, Rojas M, Willis M, Leask A, *et al*: Wnt1/β catenin injury response activates the epicardium and cardiac fibroblasts to promote cardiac repair. EMBO J 31: 429-442, 2012.
44. Boudreau RL, Spengler RM and Davidson BL: Rational design of therapeutic siRNAs: minimizing off-targeting potential to improve the safety of RNAi therapy for Huntington's disease. Mol Ther 19: 2169-2177, 2011.
45. Scaggiante B, Dapas B, Farra R, Grassi M, Pozzato G, Giansante C, Fiotti N and Grassi G: Improving siRNA bio-distribution and minimizing side effects. Curr Drug Metab 12: 11-23, 2011.